AIAA AVIATION Forum
12-16 June 2023, San Diego, CA and Online
AIAA AVIATION 2023 Forum

10.2514/6.2023-3524

An Experimental Study to Characterize the Effects of Ice Accretion on the Aerodynamic Performance of an Offshore Wind Turbine Blade Model

Harsha Sista[1], Haiyang Hu[2], and Hui Hu[3]

Department of Aerospace Engineering, Iowa State University, 1200 Howe Hall, 537 Bissell Road, Ames, IA, 50011-1096, USA

Abstract

The accretion of ice on the surface of a wind turbine blade causes a drastic reduction in the aerodynamic performance and as a result, the power output, in addition to posing a safety hazard. To quantify this phenomenon, an experimental study was conducted in the Iowa State University Icing Research Tunnel (ISU-IRT) to understand the dynamic ice accretion process and resultant aerodynamic performance degradation specifically experienced by offshore wind turbines at higher Liquid Water Content (LWC) levels. Four different LWC values were tested for both glaze and rime ice conditions each, to cover the possible spectrum of typical icing conditions. A high-speed imaging camera was used to capture the dynamic ice accretion process, while a Digital Image Projection (DIP) technique was used to perform the 3D qualification of the ice accretion characteristics. Two highly sensitive multi-axis force and moment transducers were used to measure the lift and drag forces acting upon the airfoil. The lift force was found to decrease, and the drag force was found to increase with the formation of ice. The amount of change in the unsteady aerodynamic forces was found to depend on the ambient temperature, the LWC, as well as the accreted ice structure.

Nomenclature

AoA	=	Angle of Attack
C	=	Chord length of the airfoil
LWC	=	Liquid Water Content
MCCS	=	Maximum Combined Cross Section
MVD	=	Median Volume Diameter of a droplet
V	=	Airflow velocity
$t(\tau)$	=	time index during the ice accretion process (s)
T	=	Temperature
x	=	spatial *x* coordinate of the airfoil
y	=	spatial *y* coordinate of the airfoil
R	=	Airfoil leading-edge radius (mm)
τ	=	Accretion time (s)
ρ_i	=	Density of ice (g/m^3)

1. Introduction

[1] PhD Student, Department of Aerospace Engineering.

[2] Post-Doctoral Researcher, Department of Aerospace Engineering.

[3] Martin C. Jischke Professor, Department of Aerospace Engineering, AIAA Associate Fellow.

Renewable energy has emerged as a viable alternative for fossil fuel-based energy in the recent past, leading to increased development of infrastructure dedicated to generating sustainable and clean energy. As a result, wind, solar, and hydroelectric power have drawn research on making them more efficient. This has made wind energy one of the fastest fastest-growing renewable energy sources in recent decades [1]. A study by the US Department of Energy has shown that by 2030, over 20% of the United States energy demand can be met by wind energy alone [2]. To fulfill this ambitious goal, there has been a massive increase in the installation of onshore wind turbines and the increase in their power production capacity. Furthermore, the White House has announced a goal of reaching 30 GW of power generated through offshore wind turbines alone, which will be enough to power 10 million homes with clean energy [3]. Therefore, ensuring that offshore wind turbines are operating at maximum capacity for as long as they can is paramount for achieving these goals.

The reason why there has been so much focus on offshore wind turbines in energy targets and research is because they have a natural and distinct advantage over their onshore counterparts [4]:

- stronger and more consistent offshore winds can result in greater power production,
- the turbine size can be significantly larger,
- offshore wind parks can be installed closer to major cities, reducing the transmission line length to deliver the power,
- the visual and auditory impact of offshore wind turbines is lesser.

However, the associated difficulties of increased installation cost, higher operation and maintenance charges, and the difficulty of year-round access to the site due to changing weather conditions can be balanced by conducting research into decreasing the downtime of these turbines [5].

The installation of wind turbines in cold climate regions has also increased. A study by Fortin [6] has found that the installation of wind turbines at higher latitudes in a northern climate results in a 10% increase in the production of power because of the increase in air density caused by colder temperatures. In a study by Lehtomaki [7], it was found that the total power generated by wind turbines in cold climates was 127 GW at the end of 2015. Therefore, a larger fraction of offshore wind turbines will be at risk of experiencing icing events (72%, 94% and 19% in North America, Europe, and Asia respectively). This is why the effect of icing events on offshore wind turbines becomes important. Ice accumulation on wind turbine blade surfaces can change their shapes and cause aerodynamic performance degradation, which can account for up to a 30% decrease in the Annual Energy Production (AEP) [8], [9]. In addition, ice accretion can also accelerate the natural corrosion process of the blade. Therefore, it is highly desirable and necessary to develop anti/de-icing techniques suitable for offshore wind turbines so that the icing-induced damage and performance degradation can be minimized, ensuring a safer operation cycle for offshore wind turbines in cold climates.

The development of icing mitigation techniques begins with gaining a comprehensive understanding of the physics involved in the icing process. This process can be classified into three distinct types: in-cloud icing, precipitation icing, and frost [10]. In-cloud icing occurs when supercooled water droplets impinge upon a surface below 0°C and freeze upon impact. Precipitation icing happens during rainy or snowy conditions and is responsible for higher ice accretion rates, even though the temperature is relatively higher. Frost deposition occurs when water vapor directly solidifies on a cold surface and is relatively rarely observed. Among these, in-cloud icing is the most prevalent and widespread form of icing and is the focus of this article.

In-cloud icing depends on a variety of factors such as ambient temperature, wind speed, blade characteristics, Liquid Water Content (LWC), and Median Volume Diameter (MVD) of the droplets. Based on these characteristics, in-cloud icing can be further divided into rime ice, glaze ice, and mixed ice. Rime ice forms at lower LWC and MVD values, usually at temperatures below -10°C. The supercooled water droplets freeze directly upon impingement, resulting in the formation of an opaque and milky layer of ice. Glaze ice forms at warmer temperatures, between 0°C to -10 °C, with higher LWC and MVD values. A glassy and clear sheet of smooth ice is formed, with some runback observed along the direction of the wind, since the entire droplet does not freeze instantly upon impingement. A combination of the conditions for rime and glaze ice result in the formation of uneven mixed ice with differing freezing rates. Out of the three, glaze ice is generally considered the most dangerous type of ice, since it can result in the formation of ice shapes which substantially alter the geometry of the accreting surface [11].

There is a gap in literature when it comes to understanding the fundamental physics involved in offshore wind turbine icing and the strategies required for icing mitigation. Previous work has been done by the author to explore the qualification of ice accretion characteristics for offshore wind turbines [12]. The two closest fields are onshore wind turbine icing studies and ice accretion studies on marine vessels, which have been used as the building blocks for this research. The process of onshore wind turbine icing has been described in the paragraphs above, but an important factor that comes into play only on offshore wind turbines is the presence of sea spray. To understand the mechanism behind sea spray icing and its consequences, literature related to icing on marine vessels is utilized. Icing on ships and other offshore structures is caused by a combination of atmospheric sources and sea spray. For ships, sea spray is the major cause, contributing between 50-90% of all marine icing, depending on the ambient weather conditions [13], [14]. For offshore wind turbines, the icing caused by atmospheric condensation and sea spray icing would be more balanced, but the underlying process will remain the same. Sea spray droplets are generated when waves impact upon offshore structures, like the hull of a ship or the tower of an offshore wind turbine. The LWC and MVD of the droplets formed in this manner were studied extensively by Ryerson [15]. The major takeaway is that for offshore structures, the LWC is significantly higher than what is found onshore (typically LWC < 2.0 g/m^3) and reach up to 20.0 g/m^3 [16]. The second differentiating factor between onshore and offshore wind turbines is the presence of salt in the generated droplets, the percentage of which can vary between 0 ~ 4.0%, depending on the ambient conditions [17]. The effect of saltwater, while being part of the broader research, is out of the scope of the present study. Therefore, the current paper focuses on understanding the dynamic ice accretion process at higher LWC values corresponding to offshore wind turbine icing by conducting a comprehensive icing tunnel testing campaign using qualitative and quantitative methods and examining the results to elucidate the underlying physics.

2. Experimental Setup

The experimental study was performed in the unique Icing Research Tunnel available at Iowa State University (i.e., ISU-IRT in short), which is a newly refurbished, research-grade, multifunctional icing research tunnel. As shown schematically in Figure 1, ISU-IRT has a test section with four optically transparent side walls and dimensions of 2.0m in length x 0.4m in width x 0.4m in height. It has a capacity of generating a maximum wind speed of 60 m/s and airflow temperature down to - 25ºC. The tunnel is cooled using a heat exchanger, which is cooled by a 30 kW compressor (Vilter^{TM}). An array of 9 pneumatic atomizers/spray nozzles (H. Ikeuchi and Co., Flat Spray BIMV Series Nozzles) were installed in a 3x3 grid at the entrance of the contraction section of ISU-IRT to generate the droplets. Pressure regulators control the mass flow rate of the water fed to the spray nozzles, which was measured using a digital flow meter (Omega, FLR-1605A), which in turn controls the LWC level inside the tunnel. The ISU-IRT is currently capable of generating LWC up to 5.0 g/m^3. By using ISU-IRT, extensive icing and anti-/de-icing studies have been carried out in recent years for various engineering applications. Further information about the ISU-IRT can be found in Gao et al. [18].

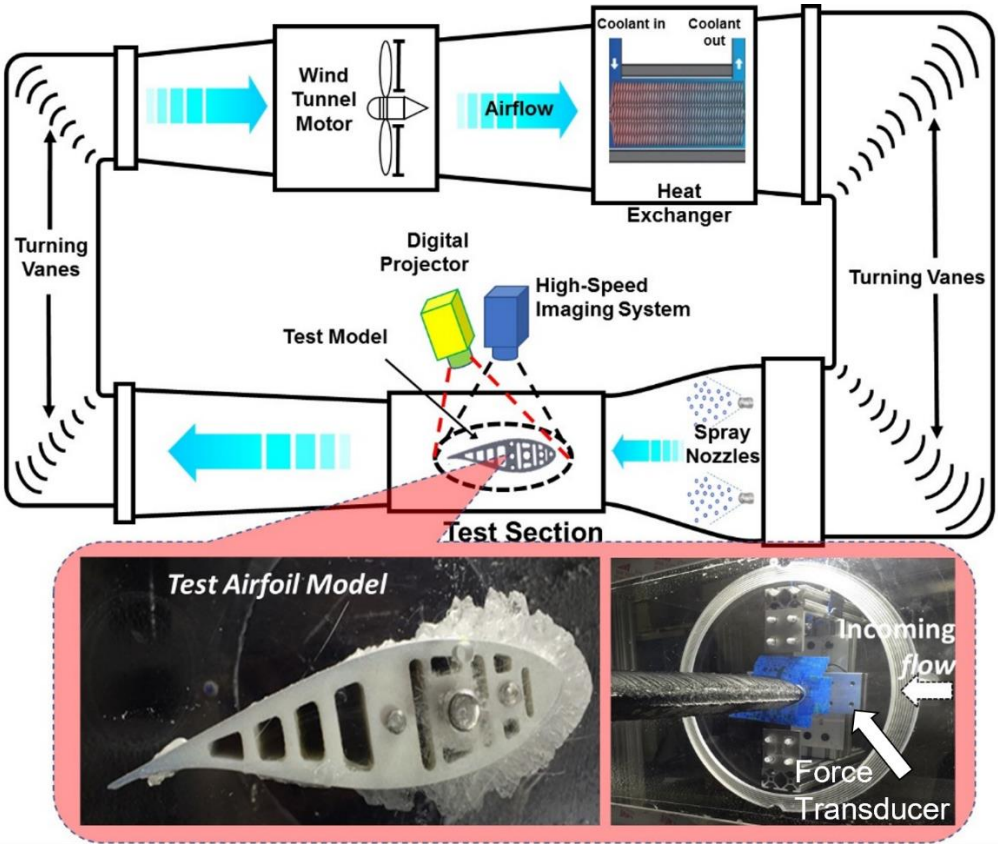

Figure 1: Schematic of the Iowa State University Icing Research Tunnel (ISU-IRT)

The airfoil model used in the experimental study is the DU91-W2-250 airfoil profile, which is widely used for wind turbine blade design due to its favorable aerodynamic performance and structural properties [19], [20]. The turbine blade model is 0.15m in airfoil chord length (i.e., C ¼ 0.15 m) and 0.40m in spanwise length. It was manufactured using a 3D printing rapid-prototyping machine. The surface of the model was sanded by using a series of progressively finer sandpapers, from 220 grit to 2000 grit, to achieve a smooth finish with a characteristic roughness of about 20-25μm [21]. Following that, several coatings of a primer were applied to prepare the surface for an all-weather spray-on enamel coating that is widely used to protect the surface of wind turbine blades (Rustoleum™, Flat Protective Enamel, white in color). The blade was mounted using three stainless-steel rods and set at an Angle of Attack of 5.0 degrees (i.e., AOA=5.0°), which coincides with the angle at which the airfoil model has its maximum lift-to-drag ratio. To simulate typical Glaze icing conditions experienced by offshore wind turbines, the initial testing parameters were set to V_∞ = 40 m/s, T_∞ = -5 ºC. Typical Rime icing conditions experienced by offshore wind turbines were also simulated, with the initial testing parameters set to V_∞ = 40 m/s, T_∞ = -15 ºC. The ice accretion was studied for eight different test cases, as shown in

Table 1:

Table 1: Test Matrix for the present study

Case Number	AoA (°)	V_∞ (m/s)	T (°C)	LWC (g/m^3)	Expected Ice Type	Runtime (s)
1	5	40	-5	0.5	Glaze	600
2	5	40	-5	1.0	Glaze	300
3	5	40	-5	2.0	Glaze	150
4	5	40	-5	4.0	Glaze	75

5	5	40	-15	0.5	Rime	600
6	5	40	-15	1.0	Rime	300
7	5	40	-15	2.0	Rime	150
8	5	40	-15	4.0	Rime	75

To capture the ice accretion process over the wind turbine blade model, a high-resolution imaging system (Photron Fastcam Mini WX Series) was mounted normal to the airfoil chord of the wind turbine model. Low-flicker illumination was provided by a set of 150W fiber-coupled halogen lamps (RPS Studio CooLED 200 RS-5620). In addition, a Digital Image Processing (DIP)-based 3-D scanning system was used to capture the ice structure formed on the wind turbine model after running the experiment. The DIP system uses the concept of structured light triangulation in a similar fashion to the stereo vision technique, with one important difference: a digital projector replaces one of the cameras in the stereo pair. This projector highlights the accreted ice structures while the camera captures the surface characteristics.

Two high-sensitivity multi-axis force-moment transducers (ATI-IA Mini 45) were mounted at either end of the blade model to capture the aerodynamic degradation by measuring the lift and the drag forces. The transducers consist of foil strain gage bridges, capable of measuring force on three axes as well as the torque about each axis. The data from the transducers was acquired by using a 16-bit NI USB-6218 data acquisition system with a frequency of 1000 Hz.

The DU-91-W2-250 airfoil was mounted inside the test section of the ISU-IRT using three stainless steel rods and set to the desired angle of attack of 5 degrees. The refrigeration system was then turned on and the ambient air inside the tunnel was cooled to the target temperature for around 20 minutes before beginning the experiment to ensure thermal a thermally steady state inside the test section. The spray nozzle system, already set at the desired Liquid Water Content, was switched on for the required time. The high-speed imaging system and the force-moment transducers were also engaged along with the spray nozzles to obtain all the necessary data.

3. Experimental Results and Discussion

3.1. Qualification of Ice Accretion Characteristics through high-speed imaging

The qualification of ice accretion characteristics at higher LWC values is explored in detail in a previous paper [12]. For the purposes of continuity and better understanding, the key results of the paper are summarized in this section. Typical Glaze Ice conditions are simulated at V_∞ = 40 m/s and T = -5°C, with the formation of glassy, transparent ice structures that do not immediately freeze upon impact [22]. This happens because the heat transfer is insufficient to remove the entirety of the latent heat of fusion released during the freezing process [23]. This volume of unfrozen water is affected by the aerodynamic shear force exerted by the boundary layer airflow and starts moving in the direction of the oncoming flow towards the trailing edge, freezing in stages along the way [24]. Therefore, this runback results in the formation of rivulet structures at higher LWC values. Typical Rime Ice conditions are also simulated at V_∞ = 40 m/s and T = -15°C, resulting in the formation of an opaque, milky white layer of ice. In this case, all of the latent heat of fusion is easily removed by heat transfer, resulting in the supercooled water droplets freezing instantly upon impingement. Four different LWC values are studied in this experimental campaign, and the Accumulation parameter A_c is kept the same to ensure that the total amount of accreted ice remains constant. The accumulation parameter is defined as [25]:

$$A_c = \frac{V \,.\, LWC \,.\, \tau}{2R \,.\, \rho_i}$$

The high-speed imaging system captures the dynamic ice accretion process over the airfoil. A slice is extracted and studied at various time instants to demonstrate the time evolution. Figure 2**Error! Reference source not found.** shows the dynamic ice accretion process for the Glaze icing condition at V_∞ = 40 m/s and T = -5°C at four different LWC values: (a) LWC = 0.5 g/m^3, (b) LWC = 1.0 g/m^3, (c) LWC = 2.0 g/m^3 and (d) LWC = 4.0 g/m^3, with a runtime of 600s, 300s, 150s, and 75s respectively:

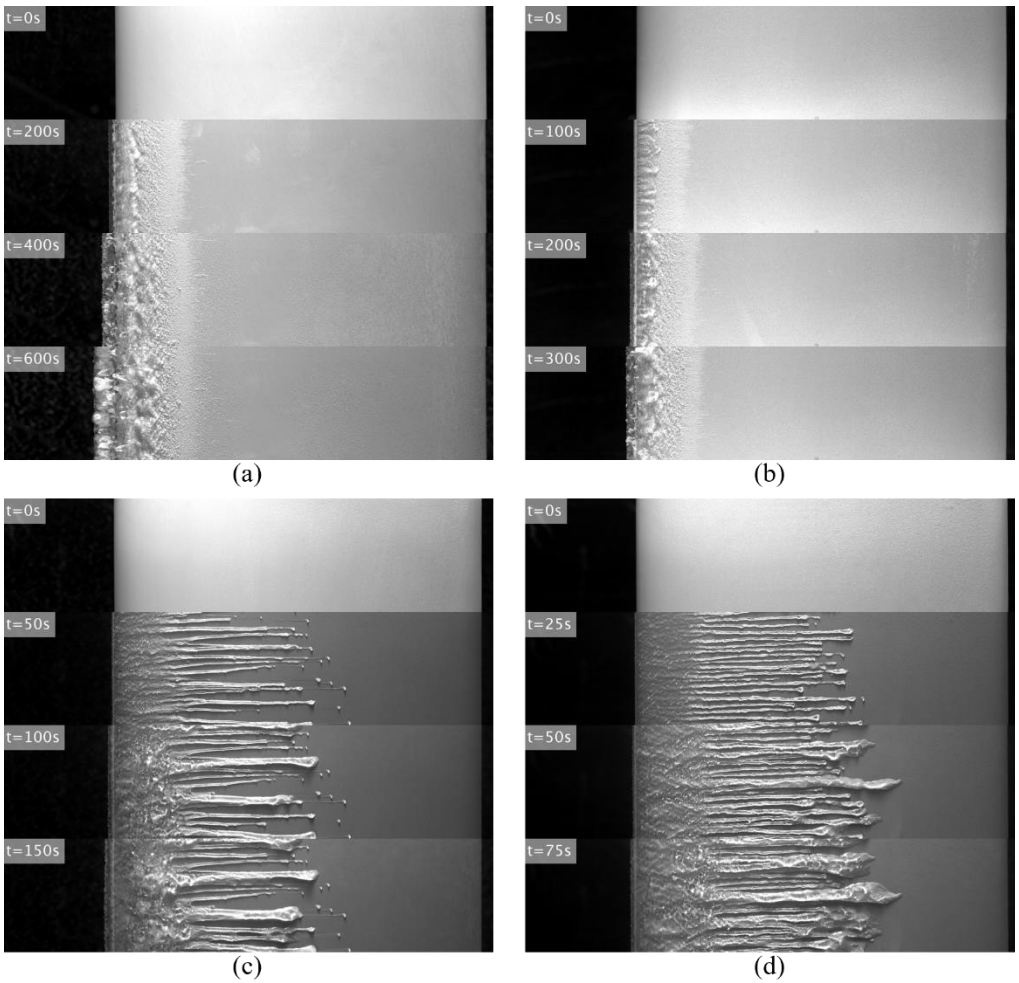

Figure 2: Dynamic Ice Accretion Process on the surface of the wind turbine blade model for Glaze Ice at V_∞ = 40 m/s, T = -5 °C at (a) LWC = 0.5 g/m^3 (b) LWC = 1.0 g/m^3 (c) LWC = 2.0 g/m^3 (d) LWC = 4.0 g/m^3

The leading-edge ice thickness, defined as the thickness of accreted ice above the leading edge of the airfoil, decreases with an increase in the LWC, as can be seen from Figure 2**Error! Reference source not found.**(a)-(d). The number and thickness of the runback rivulets also correspondingly increases, and the distribution of ice changes as a result. Figure 3 shows the dynamic ice accretion process for the Rime icing condition at V_∞ = 40 m/s and T = -15°C at four different Liquid Water Contents: (a) LWC = 0.5 g/m^3, (b) LWC = 1.0 g/m^3, (c) LWC = 2.0 g/m^3 and (d) LWC = 4.0 g/m^3, with a runtime of 600s, 300s, 150s and 75s respectively. Milky, opaque deposits of ice are observed to form on and above the leading edge, and in this case as well, the trend of the leading-edge ice thickness decreasing with an increase in the LWC holds true, as can be seen from Figure 3(a)-(d).

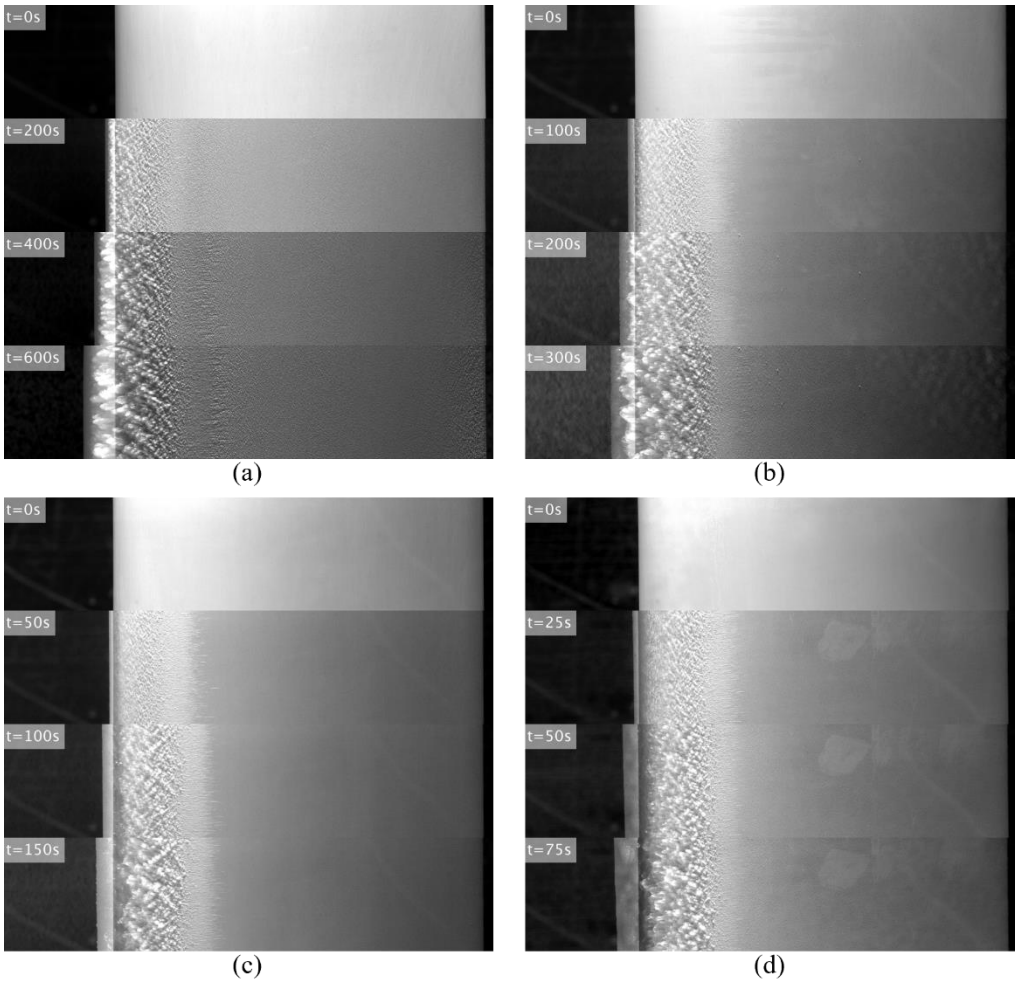

Figure 3: Dynamic Ice Accretion Process on the surface of the wind turbine blade model for Rime Ice at V_∞ = 40 m/s, T = -15 °C at (a) LWC = 0.5 g/m^3 (b) LWC = 1 g/m^3 (c) LWC = 2 g/m^3 (d) LWC = 4 g/m^3

Once the experiment was completed, the iced model was transported to a cooling chamber cooled to -10 °C, where a Digital Image Projection (DIP) based 3-D scanning setup was installed, more details of which can be found in Gao et al. [26]. A calibration was done before beginning this process to establish a correlation between the digital projector and the high-resolution camera. 90 2D scans were combined into a 3D model to provide accurate qualitative data. Figure 4 compares the ice accretion for the Glaze ice cases, while Figure 5 compares the ice accretion for the Rime ice cases. The change in the leading-edge ice thickness for the four different cases for both temperatures and the ice accretion characteristics in the spanwise and chordwise directions can also be clearly observed from the 3D scan results. Figure 5 (d) is of particular interest as it depicts uneven ice accretion due to different freezing fractions of glaze and rime ice.

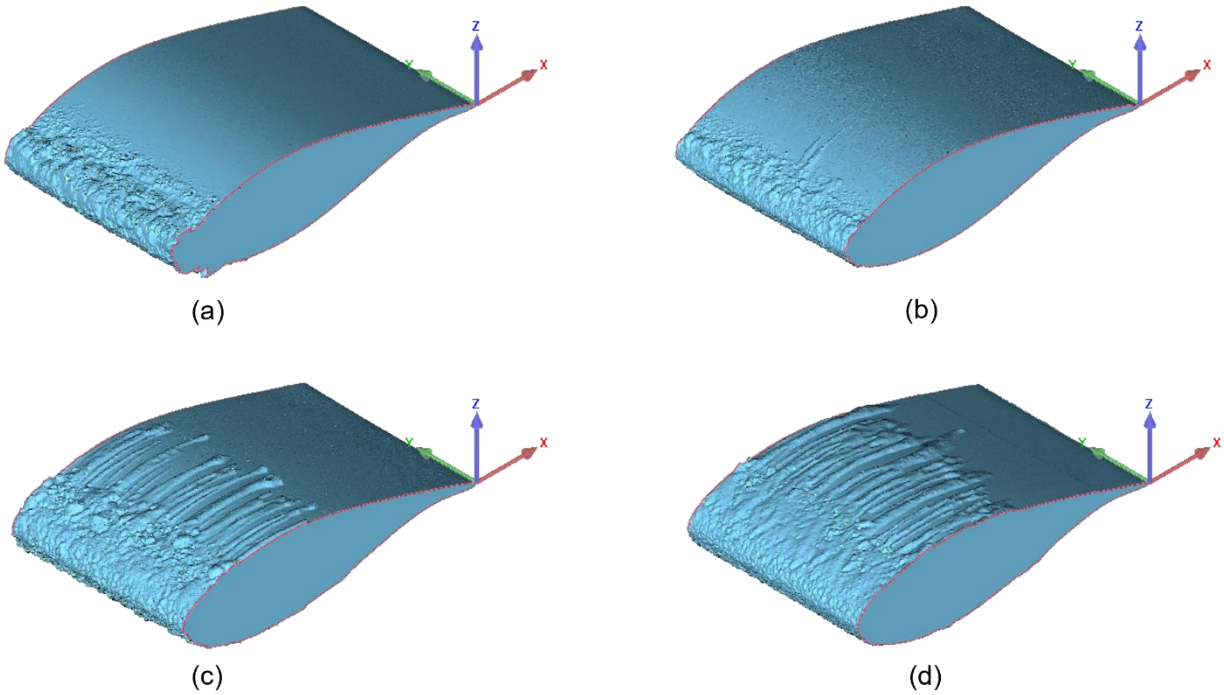

Figure 4: 3D Shape of the accreted ice on the surface of the wind turbine blade model for Glaze Ice at V = 40 m/s, T = -5 °C at (a) LWC = 0.5 g/m^3 (b) LWC = 1.0 g/m^3 (c) LWC = 2.0 g/m^3 (d) LWC = 4.0 g/m^3

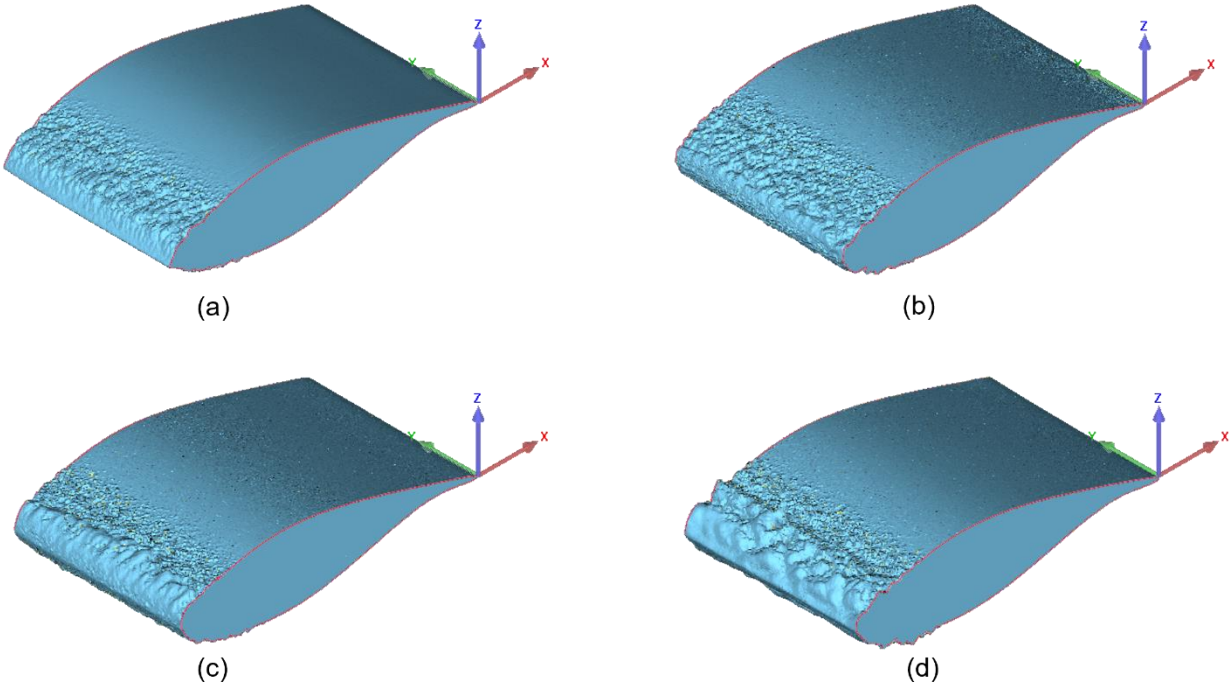

Figure 5: 3D Shape of the accreted ice on the surface of the wind turbine blade model for Rime Ice at V = 40 m/s, T = -15 °C at (a) LWC = 0.5 g/m^3 (b) LWC = 1.0 g/m^3 (c) LWC = 2.0 g/m^3 (d) LWC = 4.0 g/m^3

2D slices are taken at four different spanwise locations and the concept of Maximum Combined Cross Section (MCCS), which is mentioned in Woodward et al. [27], is used to acquire a comparison of how the ice shape depends on the LWC. The MCCS is obtained by taking the maximum outer boundary profile from the superimposed 2D sections. The MCCS from each of the four Glaze ice cases and each of the four Rime ice cases are then superimposed in a single graph, as shown in Figure 6:

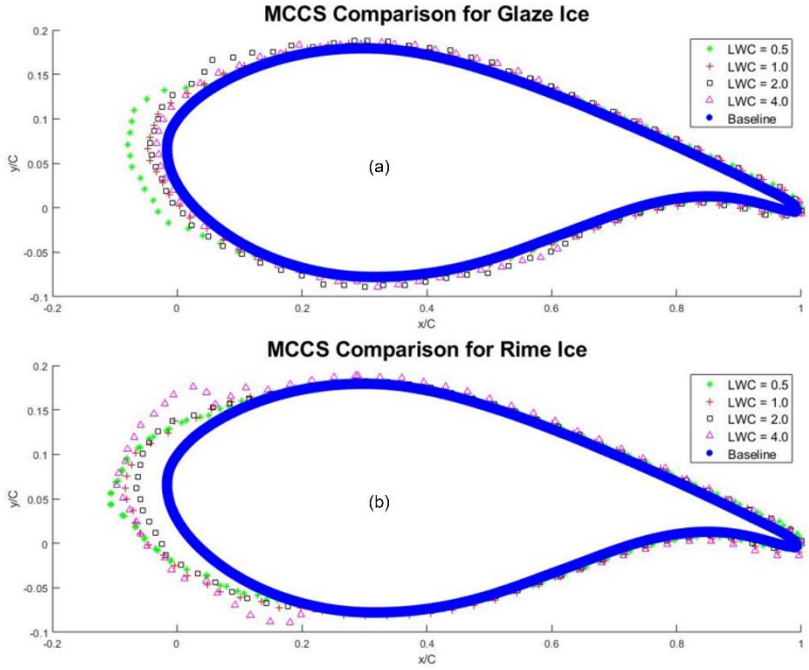

Figure 6: Comparison of the MCCS for different Liquid Water Contents for (a) Glaze Ice and (b) Rime Ice

From Figure 6 (a), we see that as the LWC increases, the leading-edge ice thickness decreases and there is more ice over the surface downstream, which is indicative of runback. A similar trend is observed in Figure 6 (b) for the rime ice condition, with the notable exception of when LWC = 4.0 g/m^3, when mixed ice formation is observed. Therefore, we can say that there is an inverse relationship between the leading-edge ice thickness and the LWC for the glaze Ice condition, except for LWC = 4.0 g/m^3 at T = -15 ℃.

3.2. Quantification of aerodynamic performance degradation during the dynamic ice accretion process

The unsteady aerodynamics forces of lift and drag are important to study during the dynamic ice accretion process since they dictate the performance of airfoils. To quantify the way these forces are affected by icing events, the lift and drag forces were measured on the mounted turbine blade using two force-moment transducers as described in section 2. The coefficients of lift and drag, which are calculated from the measured lift and drag forces, are normalized by the respective values measured when the airfoil was ice free on the y-axis, while the accumulation parameter defined in section 2 was normalized on the x-axis to ensure the same bounds for all 8 cases. These normalized results are plotted in Figure 7 and Figure 8Figure 8 for glaze and rime ice respectively:

Once the spray system is engaged, there is a rapid decrease in the lift force and a rapid increase in the drag force in the initial stages of the experiment. The rate of decrease of lift tapers off towards moderation as time goes on while and rate of increase of drag is more volatile. This initial effect, which can be observed for all cases, is explained by the formation of an initial rough ice structure which changes the geometry of the airfoil and disturbs the attached flow, possibly causing it to separate. The graphs diverge in terms of the magnitude of this decrease, and the rate at which the decrease happens, which can be explained by the icing structure characteristics corresponding to each case.

In Figure 7(a), the coefficient of lift follows the trend: LWC 0.5>LWC 4.0>LWC 1.0> LWC 2.0 while in Figure 7(b), the coefficient of drag follows the trend: LWC 2.0>LWC 1.0> LWC 0.5> LWC 4.0. The degradation of lift and increase in drag depends on multiple factors: the change in shape at the leading edge of the airfoil and the change in surface roughness of the accreted ice structure. From Figure 4, we can see that case (c) has both ice formation on the leading edge, and significant rivulet formation. Therefore, the degradation in terms of lift and drag is the worst for this case (~40% and ~55% respectively). This case is followed by LWC = 1.0 g/m^3, which has no rivulet formation, but the change in leading edge geometry due to the accreted ice is significant. It is interesting to note that for LWC = 0.5 g/m^3, the leading-edge ice thickness is greater, but the aerodynamic performance degradation is lesser. This can be explained by the greater increase in the effective chord length of the iced airfoil, not considering which would increase the value of the coefficients of lift and drag. When it comes to LWC = 4.0 g/m^3, leading-edge ice thickness is much smaller, and most of the degradation in the latter part of the graph is caused by the rivulets, leading to the amount of drag being much lesser than the other three (~30% degradation), even though the lift is comparable (~35% degradation).

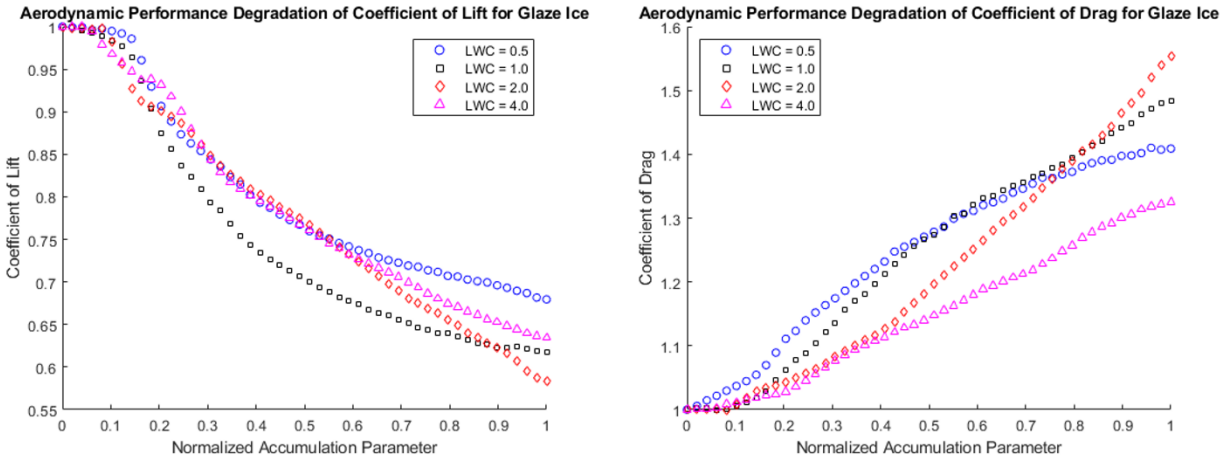

Figure 7: Aerodynamic Performance Degradation of the airfoil due to the dynamic glaze ice accretion process in terms of (a) Coefficient of Lift and (b) Coefficient of Drag

In Figure 8(a), the coefficient of lift follows the trend: LWC 2.0 ~ LWC 0.5> LWC 1.0> LWC 4.0, while in Figure 8(b), the coefficient of drag follows the trend: LWC 4.0> LWC0.5> LWC 1.0 ~ LWC 2.0. As we can see, the LWC = 4.0 g/m^3 case is clearly an outlier because of the formation of mixed ice and the details discussed above. The ice profile evident in Figure 5(d) explains how significantly the geometry of the airfoil and the surface roughness of the iced surface change. This in turn causes a high amount of degradation in the coefficients of lift and drag for this case (~50% and 65% respectively). For the other three cases, the final values of both coefficients are close, with ~ 35% decrease in lift and ~ 30% increase in drag. However, for LWC = 0.5 g/m^3, the initial decrease in lift and increase in drag are greater, because all the ice accretes on the leading edge and changes the shape of the airfoil drastically. The extension of the chord length of the airfoil and the resultant increase in the coefficients of lift and drag is maximum for LWC = 0.5g/m^3.Therefore, we see that for both glaze and rime ice, the aerodynamic performance degradation is not just a function of the leading-edge ice thickness and the change in effective chord length,but also of the kind of structure formed on the surface.

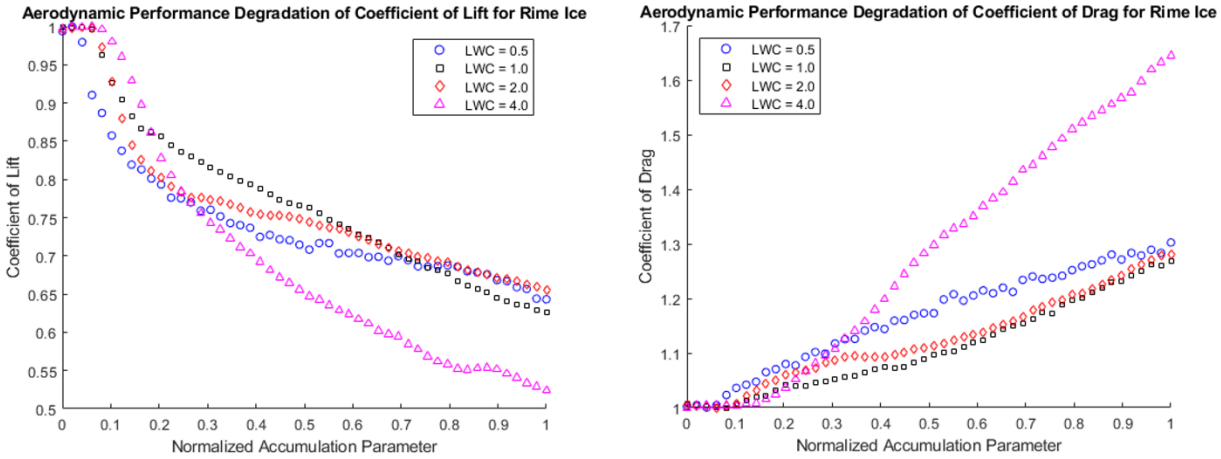

Figure 8: Aerodynamic Performance Degradation of the airfoil due to the dynamic rime ice accretion process in terms of (a) Coefficient of Lift and (b) Coefficient of Drag

4. Conclusions

The research idea for the present study was to conduct a comprehensive experimental investigation to understand and elucidate the icing physics for high Liquid Water Content icing conditions. The experiments were conducted in the Icing Research Tunnel at Iowa State University (ISU-IRT), using the DU-91-W2-250 airfoil as the wind turbine model. 8 test cases were performed: 4 for Glaze ice and 4 for Rime ice at varying Liquid Water Content (LWC) values to cover the typical icing conditions expected to be found for offshore wind turbines. The dynamic ice accretion process for each case was captured using a high-speed imaging camera, and a Digital Image Projection (DIP) based 3D scanning system was used to qualitatively visualize the ice structure formed for each case. 2D slices were extracted along the spanwise length and then superimposed over each other to visualize the ice thickness with respect to the non-iced baseline case. The Maximum Combined Cross Section (MCCS) was then calculated for each case, and the curves from the four glaze and four rime ice cases were compared to understand the relationship of ice accretion with respect to the Liquid Water Content. The leading-edge ice thickness was found to be an important parameter through this part of the study, with a decreasing trend emerging with an increase in the LWC, for both glaze and rime ice conditions. Rime ice at LWC = 4.0 g/m^3 was found to be a notable exception, both in terms of the accreted ice geometry along the leading edge and in the spanwise direction due to the formation of irregular mixed ice. This qualification of the ice structure characteristics on the wind turbine blade model is beneficial in improving our understanding of the physics involved in icing events pertinent to offshore wind turbines.

To quantify the effect such ice accretion had on the aerodynamic performance of the wind turbine airfoil, force-moment transducers were used to measure the lift and drag as the experiment was performed. This time series of data was converted to the coefficients of lift and drag and normalized and plotted in terms of the normalized accumulation parameter. This ensured that we could perform a comparison of the degradation of lift and increase of drag as the ice accretion process took place. For glaze ice, the leading-edge ice thickness and the effect of rivulet formation combined to influence the aerodynamic performance. For rime ice, the geometry change of the leading edge played more of a role, with the exception of the LWC = 4.0 g/m^3 case, which performed the worst. Therefore, the aerodynamic performance degradation does not follow the same correlation as the leading-edge ice thickness but is a more complex process dependent on other factors such as the surface roughness of the accreted ice.

While this study builds up on several previous experimental studies carried out to characterize wind turbine icing, this is believed to be the first to focus exclusively on the conditions typically found in regions where offshore wind turbines are installed. The results of this study can be used to predict the kind of ice formation for a given set of conditions and can act as the first step for further studies to develop effective anti/de-icing strategies targeted to mitigating the harmful effects of ice accretion on offshore wind turbine blades.

Acknowledgements

This research work is partially supported by Iowa Energy Center for Wind Turbine Icing Study under the IEC Competitive Grant #312350 and National Science Foundation (NSF) under award numbers OISE-1826978, CBET1916380, and TI-2140489.

References

[1] M. Grujicic, G. Arakere, B. Pandurangan, V. Sellappan, A. Vallejo, and M. Ozen, "Multidisciplinary design optimization for glass-fiber epoxy-matrix composite 5 MW horizontal-axis wind-turbine blades," *J Mater Eng Perform*, vol. 19, no. 8, pp. 1116–1127, Nov. 2010, doi: 10.1007/S11665-010-9596-2/FIGURES/12.

[2] "20% Wind Energy by 2030: Increasing Wind Energy's Contribution to U.S. Electricity Supply", Accessed: Mar. 04, 2023. [Online]. Available: http://www.osti.gov/bridge

[3] "FACT SHEET: Biden Administration Jumpstarts Offshore Wind Energy Projects to Create Jobs | The White House." https://www.whitehouse.gov/briefing-room/statements-releases/2021/03/29/fact-sheet-biden-administration-jumpstarts-offshore-wind-energy-projects-to-create-jobs/ (accessed Mar. 04, 2023).

[4] S. P. Breton and G. Moe, "Status, plans and technologies for offshore wind turbines in Europe and North America," *Renew Energy*, vol. 34, no. 3, pp. 646–654, Mar. 2009, doi: 10.1016/J.RENENE.2008.05.040.

[5] G. van Bussel, G. van Bussel, M. Zaaijer, and M. Sc, "Reliability, Availability and Maintenance aspects of large-scale offshore wind farms, a concepts study Characterisation and modeling of active and passive airfoil add-on's View project Reliability, Availability and Maintenance aspects of large-scale offshore wind farms, a concepts study," 2001, Accessed: May 01, 2022. [Online]. Available: https://www.researchgate.net/publication/239589238

[6] G. Fortin Bombardier and J. Perron, "Behaviour and Modeling of Cup Anemometers under Icing Conditions Modeling and simulation of the effects of icing on the performance of wind turbines View project AirStorage : Wind-Diesel Systems with Compressed Air Energy Storage View project," 2005, Accessed: Mar. 05, 2023. [Online]. Available: https://www.researchgate.net/publication/259758149

[7] V. Lehtomäki, "Wind Energy in Cold Climates Available Technologies-report," 2016.

[8] F. Lamraoui, G. Fortin, R. Benoit, J. Perron, and C. Masson, "Atmospheric icing impact on wind turbine production," *Cold Reg Sci Technol*, vol. 100, pp. 36–49, Apr. 2014, doi: 10.1016/J.COLDREGIONS.2013.12.008.

[9] F. Feng, S. Li, Y. Li, and W. Tian, "Numerical simulation on the aerodynamic effects of blade icing on small scale Straight-bladed VAWT," *Phys Procedia*, vol. 24, pp. 774–780, Jan. 2012, doi: 10.1016/J.PHPRO.2012.02.115.

[10] O. Parent and A. Ilinca, "Anti-icing and de-icing techniques for wind turbines: Critical review," *Cold Reg Sci Technol*, vol. 65, no. 1, pp. 88–96, Jan. 2011, doi: 10.1016/J.COLDREGIONS.2010.01.005.

[11] G. Fortin and J. Perron, "Wind Turbine Icing and De-Icing," 2009, doi: 10.2514/6.2009-274.

[12] H. Sista, H. Hu, L. Tian, and H. Hu, "Qualification of Ice Accretion Characteristics on a Wind Turbine Blade Model at High Liquid Water Content Levels Pertinent to Offshore Wind Turbine Icing Phenomena," *AIAA AVIATION 2022 Forum*, 2022, doi: 10.2514/6.2022-4070.

[13] S. Mintu, D. Molyneux, and D. Oldford, "State-of-the-Art Review of Research on Ice Accretion Measurements and Modelling," *Arctic Technology Conference 2016*, Oct. 2016, doi: 10.4043/27422-MS.

[14] T. Rashid, H. A. Khawaja, and K. Edvardsen, "Review of marine icing and anti-/de-icing systems," *https://doi.org/10.1080/20464177.2016.1216734*, vol. 15, no. 2, pp. 79–87, 2016, doi: 10.1080/20464177.2016.1216734.

[15] C. C. Ryerson, Ryerson, and C. C., "Superstructure spray and ice accretion on a large U.S. Coast Guard cutter," *AtmRe*, vol. 36, no. 3, pp. 321–337, 1995, doi: 10.1016/0169-8095(94)00045-F.

[16] S. A. Mintu, D. Molyneux, and B. Colbourne, "Ship-Wave Impact Generated Sea Spray: Part 1 — Formulating Liquid Water Content and Spray Cloud Duration," *Proceedings of the International Conference on Offshore Mechanics and Arctic Engineering - OMAE*, vol. 6A-2020, Dec. 2020, doi: 10.1115/OMAE2020-18223.

[17] G. F. N. Cox and W. F. Weeks, "Salinity Variations in Sea Ice," *Journal of Glaciology*, vol. 13, no. 67, pp. 109–120, 1974, doi: 10.3189/S0022143000023418.

[18] L. Gao, Y. Liu, L. Ma, and H. Hu, "A hybrid strategy combining minimized leading-edge electric-heating and superhydro-/ice-phobic surface coating for wind turbine icing mitigation," *Renew Energy*, vol. 140, pp. 943–956, Sep. 2019, doi: 10.1016/J.RENENE.2019.03.112.

[19] W. A. Timmer and R. P. J. O. M. van Rooij, "Summary of the Delft University Wind Turbine Dedicated Airfoils," *J Sol Energy Eng*, vol. 125, no. 4, pp. 488–496, Nov. 2003, doi: 10.1115/1.1626129.

[20] R. P. J. O. M. van Rooij and W. A. Timmer, "Roughness Sensitivity Considerations for Thick Rotor Blade Airfoils," *J Sol Energy Eng*, vol. 125, no. 4, pp. 468–478, Nov. 2003, doi: 10.1115/1.1624614.

[21] L. Gao, Y. Liu, W. Zhou, and H. Hu, "An experimental study on the aerodynamic performance degradation of a wind turbine blade model induced by ice accretion process," *Renew Energy*, vol. 133, pp. 663–675, Apr. 2019, doi: 10.1016/J.RENENE.2018.10.032.

[22] R. M. Waldman and H. Hu, "High-Speed Imaging to Quantify Transient Ice Accretion Process over an Airfoil," *https://doi.org/10.2514/1.C033367*, vol. 53, no. 2, pp. 369–377, Aug. 2015, doi: 10.2514/1.C033367.

[23] Y. Liu and H. Hu, "An experimental investigation on the unsteady heat transfer process over an ice accreting airfoil surface," *Int J Heat Mass Transf*, vol. 122, pp. 707–718, Jul. 2018, doi: 10.1016/J.IJHEATMASSTRANSFER.2018.02.023.

[24] K. Zhang, T. Wei, and H. Hu, "An experimental investigation on the surface water transport process over an airfoil by using a digital image projection technique," *Exp Fluids*, vol. 56, no. 9, pp. 1–16, Sep. 2015, doi: 10.1007/S00348-015-2046-Z/FIGURES/14.

[25] D. N. Anderson, D. B. Hentschel, and G. A. Ruff, "Measurement and Correlation of Ice Accretion Roughness," 2003, Accessed: Mar. 12, 2023. [Online]. Available: http://www.sti.nasa.gov

[26] L. Gao, • Ramsankar Veerakumar, Y. Liu, and H. Hu, "Quantification of the 3D shapes of the ice structures accreted on a wind turbine airfoil model", doi: 10.1007/s12650-019-00567-4.

[27] B. S. Woodard, A. P. Broeren, S. Lee, C. W. Lum, and M. B. Bragg, "Summary of ice shape geometric fidelity studies on an iced swept wing," *2018 Atmospheric and Space Environments Conference*, 2018, doi: 10.2514/6.2018-3494.